

# Ion concentration dynamics as a mechanism for neuronal bursting

Ernest Barreto · John R. Cressman

Received: 26 August 2010 / Accepted: 13 December 2010 /  
Published online: 11 January 2011  
© Springer Science+Business Media B.V. 2011

**Abstract** We describe a simple conductance-based model neuron that includes intra- and extracellular ion concentration dynamics and show that this model exhibits periodic bursting. The bursting arises as the fast-spiking behavior of the neuron is modulated by the slow oscillatory behavior in the ion concentration variables and vice versa. By separating these time scales and studying the bifurcation structure of the neuron, we catalog several qualitatively different bursting profiles that are strikingly similar to those seen in experimental preparations. Our work suggests that ion concentration dynamics may play an important role in modulating neuronal excitability in real biological systems.

**Keywords** Neuron · Potassium · Sodium · Ion concentration · Burst · Seizure · Epilepsy

## 1 Introduction

The Hodgkin–Huxley equations [1] are of fundamental importance in theoretical neuroscience. These equations assume that the intra- and extracellular ion concentrations of sodium and potassium are constant. While this may be a reasonable assumption for the squid giant axon preparation (for which the equations were originally developed), its validity in other cases is not clear. In the mammalian brain, for example, the neurons are much smaller and they are more tightly packed, resulting in significantly smaller intra- and extracellular volumes. Thus, typical ionic currents can have a much larger effect on the ion concentrations in this case.

The effects of extracellular potassium ( $[K]_o$ ) accumulation on neuronal excitability have long been recognized [2–5], and deficiencies in  $[K]_o$  regulation have been implicated in

---

E. Barreto (✉) · J. R. Cressman  
Center for Neural Dynamics, Department of Physics & Astronomy,  
and The Krasnow Institute for Advanced Study, George Mason University,  
Fairfax, VA 22030, USA  
e-mail: ebarreto@gmu.edu

various types of epilepsy (for a review, see [6]) and spreading depression [7, 8]. More recently, computational studies have begun to clarify the role of impaired  $[K]_o$  regulation [9–15] as well as other varying ion concentrations [16, 17].

In this work, we consider from a dynamical systems perspective the role of ion concentration dynamics in the generation of periodic bursting behavior. To emphasize the generality of our approach, we base our model on the standard Hodgkin–Huxley equations. We augment these with additional equations that describe the dynamics of both intra- and extracellular sodium and potassium. The inclusion of sodium is relatively novel and plays a crucial role in the dynamics described here. We also include terms describing pumps, extracellular diffusion, and a simple glial buffering system. A different analysis of this system was presented in [18].

## 2 Model

We begin by explicitly adopting the standard convention that an outward membrane current is defined as being positive [19]. Thus, the membrane potential  $V$  is given by

$$C \frac{dV}{dt} = -I_{membrane} \tag{1}$$

where  $I_{membrane}$  represents the sum of the various membrane currents. We aim in this work to consider a very simple and general model neuron. Hence we include only the standard Hodgkin-Huxley sodium current (with instantaneous activation), the delayed-rectifier potassium current, and leak current. We write the latter in terms of separate sodium, potassium, and chloride contributions [16]. Thus,

$$\begin{aligned} I_{membrane} &= I_{Na} + I_K + I_{Cl} \\ I_{Na} &= g_{Na}[m_\infty]^3 h (V - E_{Na}) + g_{NaL} (V - E_{Na}) \\ I_K &= g_K n^4 (V - E_K) + g_{KL} (V - E_K) \\ I_{Cl} &= g_{ClL} (V - E_{Cl}), \end{aligned} \tag{2}$$

where the  $g_i$  ( $i = Na, K, Cl$ ) are maximum conductances. Time is measured in milliseconds, voltage in millivolts, and  $C, I,$  and  $g$  are measured in units per unit of membrane area, i.e.,  $\mu F/cm^2, \mu A/cm^2,$  and  $mS/cm^2,$  respectively. The reversal potentials  $E_i$  are given in terms of the instantaneous intra- and extracellular ion concentrations by Nernst equations:

$$\begin{aligned} E_{Na} &= 26.64 \ln \left( \frac{[Na]_o}{[Na]_i} \right) \\ E_K &= 26.64 \ln \left( \frac{[K]_o}{[K]_i} \right). \end{aligned} \tag{3}$$

We fix  $E_{Cl} = -81.9386$  mV.

The extracellular potassium and intracellular sodium concentration dynamics are given by

$$\begin{aligned} \tau \frac{d[K]_o}{dt} &= \gamma\beta I_K - 2\beta \tilde{I}_{\text{pump}} - \tilde{I}_{\text{glia}} - \tilde{I}_{\text{diffusion}} \\ \tau \frac{d[Na]_i}{dt} &= -\gamma I_{Na} - 3\tilde{I}_{\text{pump}}, \end{aligned} \tag{4}$$

where the concentrations are measured in millimolar.  $\gamma = 4.45 \times 10^{-2}$  is a unit conversion factor that converts the membrane currents into millimolars per second (see [Appendix](#)), and  $\beta = 7$  is the ratio of the intracellular to extracellular volume [17]. The terms with tildes are the molar currents (millimolars per second) given below, and  $\tau = 10^3$  balances the time units.

The pump, glia, and diffusion molar currents are given by

$$\begin{aligned} \tilde{I}_{\text{pump}} &= \rho \left( 1 + \exp\left(\frac{25 - [Na]_i}{3}\right) \right)^{-1} \left( \frac{1}{1 + \exp(5.5 - [K]_o)} \right) \\ \tilde{I}_{\text{glia}} &= G \left( 1 + \exp\left(\frac{18 - [K]_o}{2.5}\right) \right)^{-1} \\ \tilde{I}_{\text{diffusion}} &= \varepsilon ([K]_o - k_{\text{bath}}). \end{aligned} \tag{5}$$

We set the default parameter values to  $\rho = 1.25$  mM/s,  $G = 66.666$  mM/s, and  $\varepsilon = 1.333$  Hz.  $k_{\text{bath}}$  represents the potassium concentration in the reservoir, i.e., the bathing solution for a slice preparation, or the vasculature *in vivo*. We set  $k_{\text{bath}} = 4$  mM for normal physiological conditions.

The intracellular potassium and extracellular sodium concentrations are obtained from the following simplifying assumptions that allow us to reduce the dimensionality of the system [18]:

$$\begin{aligned} [K]_i &= 140 \text{ mM} + (18 \text{ mM} - [Na]_i) \\ [Na]_o &= 144 \text{ mM} - \beta ([Na]_i - 18 \text{ mM}). \end{aligned} \tag{6}$$

The first assumption is that the sodium membrane current is the dominant means by which sodium is transported across the membrane, and that during the course of an action potential, the transport of sodium and potassium are simply related. The second assumption is that the total amount of sodium is conserved.

The remaining parameters and the equations for the gating variables are given in the [Appendix](#).

### 3 Results

#### 3.1 Fixed ion concentrations

We begin with a discussion of the dynamical structure of our model subject to constant values of the ion concentrations. That is, we set  $[K]_o$  and  $[Na]_i$  to fixed predetermined values and obtain the remaining concentrations using (6). We then examine the behavior of the neuron as given by (1–3).

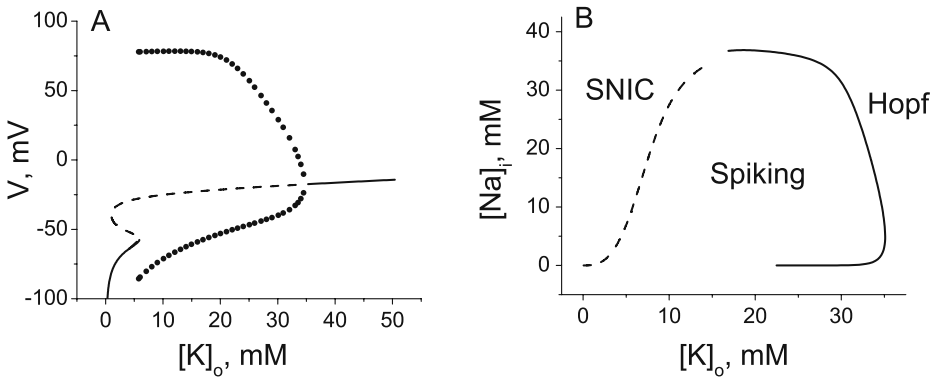


**Fig. 1** Bifurcation diagrams describing the neuron's asymptotic behavior with fixed ion concentrations. In **a**  $[Na]_i = 10$  mM. The detailed structure in the *upper part* of **b** is shown in Fig. 5

Figure 1 shows bifurcation diagrams obtained under these conditions. The features in these diagrams clarify the neuron's bursting behavior as the ion concentrations undergo slow oscillations, as explained below.

Figure 1a is constructed by holding  $[Na]_i$  fixed at 10 mM and plotting the asymptotic values of the membrane potential  $V$  versus several fixed values of  $[K]_o$ . Below approximately 5.7 mM, the neuron is attracted to a stable equilibrium (shown as a solid line) that corresponds to the resting state. At approximately  $[K]_o = 5.7$  mM, this equilibrium coalesces with a coexisting unstable equilibrium (dashed line) in a saddle-node bifurcation that occurs on an invariant closed curve (of infinite period) that appears simultaneously. This scenario is known as a saddle-node on invariant circle (SNIC) bifurcation.<sup>1</sup> Beyond this, for values of  $[K]_o$  between 5.7 and 35.2 mM, a stable limit cycle appears, reflecting regular spiking in the neuron. This is depicted in the diagram by filled circles that mark the maximum and minimum values of the membrane voltage during a cycle. For increasing values of  $[K]_o$  approaching  $[K]_o = 35.2$  mM from below, the amplitude of this periodic orbit decreases and the orbit eventually merges with the coexisting unstable equilibrium in a supercritical Hopf bifurcation. For  $[K]_o > 35.2$  mM, a stable equilibrium is found—this is the state of depolarization block [20].

Figure 1b is a two-dimensional bifurcation diagram which shows the location of the SNIC and Hopf bifurcations as the value of  $[Na]_i$  is varied. These curves delineate the boundaries of different attracting behaviors of the neuron. To the left of the SNIC curve, the neuron is attracted to the resting equilibrium. Between the SNIC and the Hopf curves, the neuron exhibits regular spiking, and to the right of the Hopf curve, the neuron is attracted to the depolarization block equilibrium. The detailed structure at the top of this diagram is discussed below.

<sup>1</sup>See, e.g., [21]. This codimension-one bifurcation has also been called a saddle-node infinite-period bifurcation [22].

### 3.2 Dynamic ion concentrations

We now describe the behavior of the full system, in which the ion concentrations are allowed to evolve dynamically. In Fig. 2, we plot the asymptotic behavior of the ion concentrations for several values of  $k_{\text{bath}}$ . Also included in the figure is a portion of the SNIC curve from Fig. 1b.

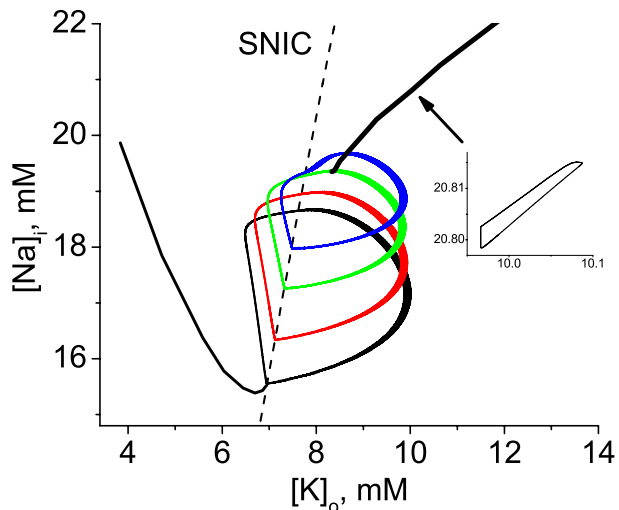
At the default parameter values described above (with  $k_{\text{bath}} = 4.0$  mM), the entire system approaches a stable equilibrium resting state for which the membrane voltage and the ion concentrations assume fixed values. As  $k_{\text{bath}}$  is increased, these equilibrium values change and sweep out the solid curve shown on the left of Fig. 2. At approximately  $k_{\text{bath}} = 7.615$  mM, this curve collides with the SNIC boundary. Just beyond this value, the system jumps to a limit cycle. As  $k_{\text{bath}}$  continues to increase, the projection of this limit cycle onto the ion concentration variables drifts upward and to the right, as shown in the figure. Henceforth, for brevity, we refer to such limit cycle projections as “loops”.

Note that these large-amplitude loops straddle the SNIC curve. In addition, they have periods on the order of several tens of seconds. Consequently, as the system alternately transitions between the resting and the spiking regions, there is ample time to exhibit those asymptotic behaviors. That is, the neuron bursts. For example, for  $k_{\text{bath}} = 8.0$  mM, the ion concentrations are attracted to the second (red) loop in Fig. 2, and the corresponding behavior of the membrane voltage is shown below in Fig. 4a.

At approximately  $k_{\text{bath}} = 9.0$  mM, the large-amplitude loop disappears. For larger  $k_{\text{bath}}$ , the ion concentrations exhibit very small-amplitude loops, as shown in the inset of Fig. 2. Since this loop lies entirely within the spiking region, the neuron exhibits tonic spiking. Indeed, the loop itself represents the small changes in the ion concentrations due to individual action potentials.

We note in passing that we have observed multistability [23–25]. For values of  $k_{\text{bath}}$  approximately in the interval (8.8, 9.0) mM, a bursting solution coexists with a tonically spiking state for the same parameter values. This is consistent with the analysis based on a reduced model in [18].

**Fig. 2** Asymptotic behavior of the ion concentrations as  $k_{\text{bath}}$  (in millimolar) is varied. The curve on the left denotes stable equilibria and corresponds to  $k_{\text{bath}}$  ranging from 4.0 to 7.615. Projections of limit cycles (loops) are shown for  $k_{\text{bath}} = 7.62, 8.0, 8.5,$  and  $8.95$  mM; the thickness of the loops on the right reflect small, fast ion concentration fluctuations due to spiking behavior. The curve on the upper right, for  $k_{\text{bath}}$  ranging from 8.8 to 15.0, denotes small-amplitude loops that correspond to tonic spiking (see inset)



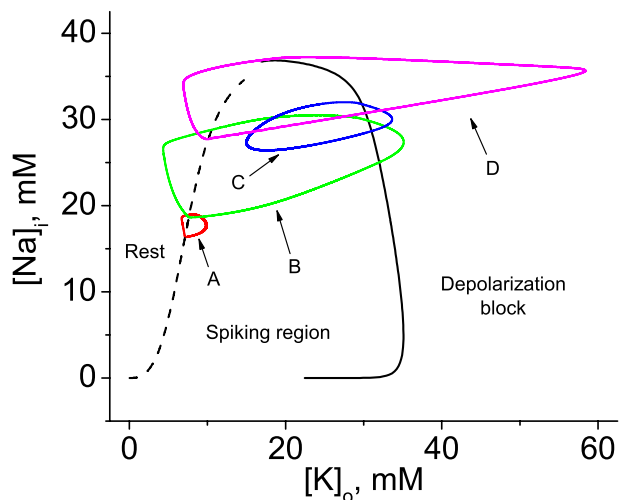
### 3.3 Catalog of bursting types

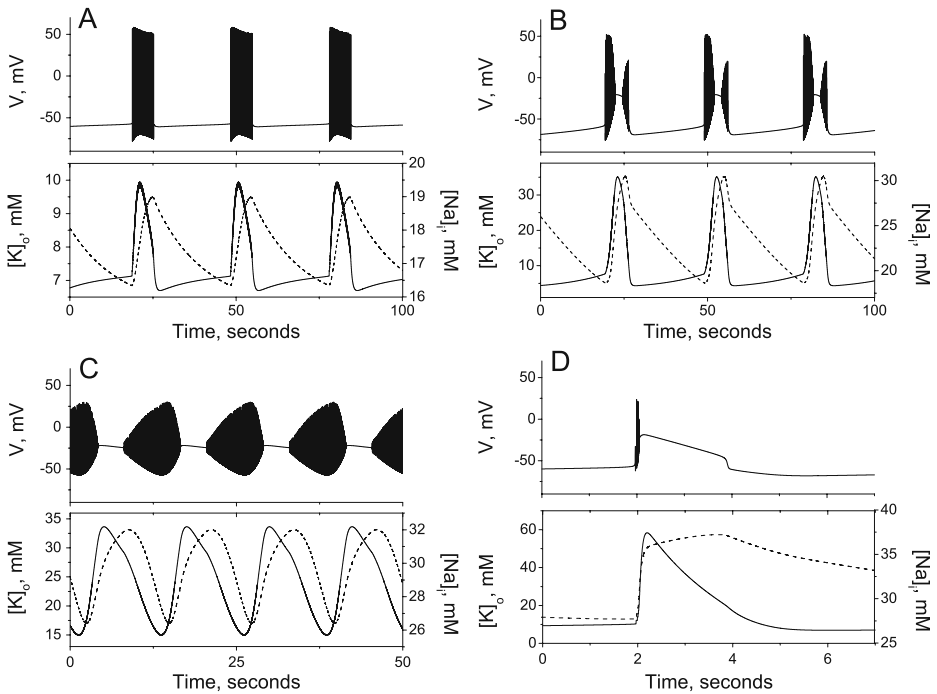
The results presented above demonstrate that for parameter values in appropriately chosen ranges, the system evolves on a limit cycle whose projection onto the ion concentration variables forms a loop that straddles the SNIC curve and the neuron bursts. Bursting behaviors of various qualitatively different kinds can be exhibited by the system if similar ion concentration loops straddle the bifurcation curves of Fig. 1b in different ways. Accordingly, we can catalog all the possible arrangements and examine the nature of the resulting bursting patterns.

Figure 3 shows four different ion concentration loops labeled A, B, C, and D. Loop A is the  $k_{\text{bath}} = 8.0$  mM loop discussed above, and the corresponding membrane voltage trace is shown in Fig. 4a. Loop B ( $G = 20$ ,  $\epsilon = 0.133$ , and  $k_{\text{bath}} = 22$ ) straddles both the SNIC and the Hopf bifurcation curves and hence displays a qualitatively different bursting pattern. As the loop is traversed, the ion concentration trajectory moves from the resting region into the spiking region by crossing the SNIC curve and then continues across the Hopf curve into the depolarization block region. It then bends around and crosses these regions in reverse order, and the cycle repeats. Consequently, the membrane potential shows a bursting pattern that moves from quiescence to spiking to depolarization block and back again, as is shown in Fig. 4b. Loop C ( $G = 6$ ,  $\epsilon = 0.7$ , and  $k_{\text{bath}} = 22$ ) straddles only the Hopf curve, and hence, the membrane potential displays round-shaped bursts, reflecting the supercritical nature of the Hopf bifurcation, as shown in Fig. 4c. Finally, loop D ( $\rho = 0.9$ ,  $G = 10$ ,  $\epsilon = 0.5$ ,  $k_{\text{bath}} = 20$ , and  $\gamma = 1.0$ ) is similar to loop B, but by examining the membrane voltage in Fig. 4d, one sees that the event termination transitions smoothly from depolarization block back to the resting level without exhibiting any spikes. This is because the return trip along the upper portion of the loop avoids the Hopf bifurcation. We clarify this transition in the next section (note that, for nearby parameter sets, it is possible to observe bursts of this type with more spikes at the event onset than are shown here).

Figure 5 shows a magnification of the upper part of Fig. 1b that reveals more detail. As the SNIC curve continues up from the lower left corner, a codimension-two bifurcation

**Fig. 3** Loops A–D represent the time evolution of the ion concentrations as the system exhibits limit cycle behavior. The loops are traversed in a counterclockwise manner. The dashed and solid lines are the SNIC and Hopf bifurcation curves, respectively





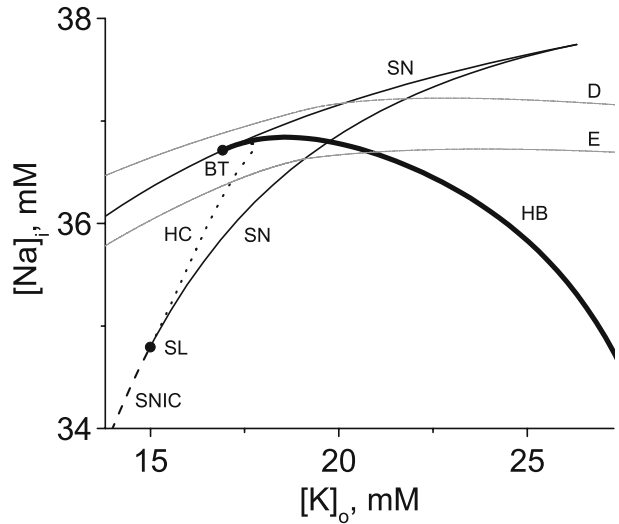
**Fig. 4** Four qualitatively different bursting patterns corresponding to the four loops shown in Fig. 3. In the lower panels, solid curves represent  $[K]_o$  (left vertical axes) and dashed curves represent  $[Na]_i$  (right vertical axes). The event in **d** recurs with a period of approximately 16.5 s, but for clarity, only a portion of one such event is shown

known as a saddle-node loop (SL) is encountered<sup>2</sup> at approximately  $([K]_o, [Na]_i) = (14.994, 34.795)$  mM. At this point, the curve splits into two branches corresponding to saddle-node (SN) and homoclinic bifurcations. The saddle-node branch continues to the upper right and forms a cusp with another saddle-node branch, while the homoclinic branch continues up, curves around, and terminates at a (codimension-two) Bogdanov–Takens (BT) point at approximately  $(16.917, 36.714)$  mM. This point is coincident with the upper SN branch and is also an endpoint of the Hopf bifurcation curve.

Superimposed on this diagram is the upper portion of loop D from Fig. 3, which represents the termination of the burst event. With the increased magnification, it can be seen that this part of the ion concentration limit cycle indeed does not cross the Hopf curve. Instead, it crosses the two saddle-node curves. To clarify the nature of the burst termination, we show in Fig. 6d the one-dimensional bifurcation diagram analogous to Fig. 1a for  $[Na]_i = 37.2$  mM, along with the burst termination portion of the system’s trajectory. Also included is an inset showing the membrane voltage versus time for one complete burst event. It can be seen that the termination (arrows) occurs when the trajectory tracking the upper stable equilibrium branch encounters the second saddle-node bifurcation and drops to the lower stable equilibrium branch.

<sup>2</sup>This bifurcation [26, 27] has also been called a saddle-node homoclinic orbit bifurcation; see [21].

**Fig. 5** Magnification of the upper portion of Fig. 1b. *D* and *E* are portions of ion concentration limit cycles as described in the text. *SN* saddle-node, *BT* Bogdanov–Takens, *HC* homoclinic, *HB* Hopf, *SL* saddle-node loop, *SNIC* saddle-node infinite period



The additional detail in Fig. 5 permits the identification of a fifth type of bursting pattern exhibited by our system (obtained with  $\rho = 0.9$ ,  $G = 10$ ,  $\epsilon = 0.5$ ,  $k_{bath} = 20$ , and  $\gamma = 0.25$ ). *E* labels the upper portion of an ion concentration loop that is slightly lower than the *D* loop. It can be seen that this portion of loop *E* crosses, in order, the Hopf, saddle-node, and homoclinic bifurcation curves. The remaining portion of loop *E* (not shown) is similar to loop *B*, and indeed, the membrane voltage traces are similar, but the termination mechanisms are different. Notably, this type of burst terminates after a few small-amplitude spikes via homoclinic rather than SNIC bifurcation; see Fig. 6e.

Finally, we note that we have also identified parameter sets that give rise to loops that encircle the *BT* point in Fig. 5 while lying entirely above the *SL* point, as well as similar loops occurring upward and to the right of this, including ones that straddle only the two *SN* curves. However, the separation of time scales is less clear in these cases. And although it might exist, we were not able to find a loop that crosses the *SNIC* and Hopf curves and then returns above the saddle-node cusp. Such a loop would exhibit a burst termination that

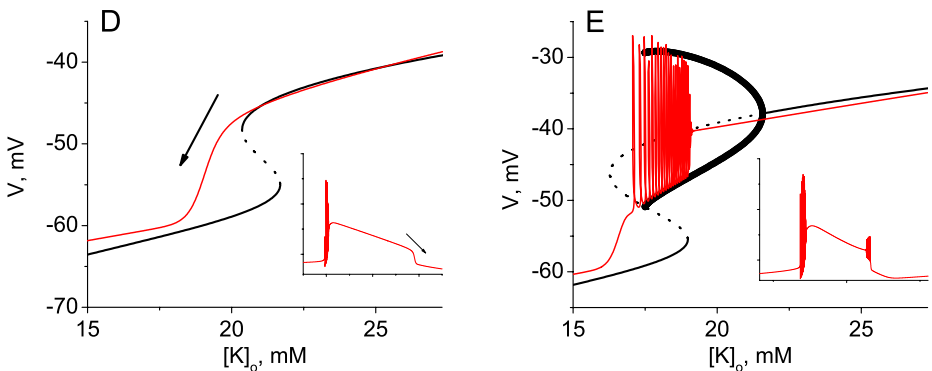


**Fig. 6** Diagrams clarifying the burst termination behavior corresponding to ion concentration loops *D* and *E* of Fig. 5. *Insets* show complete burst time traces of the membrane voltage. In *d*,  $[Na]_i = 37.2$  mM; in *e*,  $[Na]_i = 36.6$  mM

transitions from depolarization block to the rest state smoothly and without a sudden drop in membrane potential.

## 4 Discussion

In this paper, we have presented a simple model of a single neuron with dynamic intra- and extracellular sodium and potassium concentrations that exhibits periodic bursting behavior. Our goal has been to present a catalog of the wide variety of qualitatively different bursting patterns exhibited by this model based on an understanding of the underlying bifurcation structure. To do this, we have taken advantage of the large separation of time scales inherent in the model: that of spikes, which occur on the order of milliseconds, and that of the bursting events, which occur on the order of tens of seconds. We have focused attention on the nature of the fast spiking dynamics by freezing the slow ion concentration variables and identifying the asymptotic behavior of the neuron under these conditions. This clarifies how oscillations in the slow variables modulate the neuron's excitability and give rise to bursting.

A crucial aspect of our model that is typically not present in comparably simple models (to our knowledge) is the inclusion of sodium concentration dynamics. Thus, we have *two* slow variables ( $[Na]_i$  and  $[K]_o$ ) instead of one, and it is therefore possible for the slow system to undergo bifurcations to oscillatory states. Analysis complementary to the work presented here, in which bifurcations in the slow dynamics are analyzed by removing the fast dynamics via averaging, has been presented in [18].

For this study, we deliberately chose a single neuron with the classic Hodgkin–Huxley ionic currents in order to focus attention on the role of the ion concentration dynamics. Consequently, some quantitative aspects of the dynamics (e.g., the value of  $[K]_o$  for the onset of depolarization block in Fig. 1a) are not directly applicable to mammalian systems. More realistic models of mammalian systems would require additional currents and a network structure with significant synaptic activity (for example, despite the intriguing similarity of Fig. 4d to phenomena observed in spreading depression, it is known that spreading depression requires persistent sodium channels [17]). In addition, the absence of synaptic background activity means that our model neuron transitions abruptly from rest directly to bursting as  $[K]_o$  increases. In a more realistic setting, we would expect to see an intervening regime of tonic spiking due to network effects before the onset of bursting.

Although our approach has concentrated on identifying all possible bursting scenarios without regard to physiological relevance, we note that bursting morphologies similar to those that we catalog here have been observed in experimental models of epilepsy, including a high-potassium model [28], a high-potassium, low-calcium model [20], and a low-magnesium 4-aminopyridine model [29]. This suggests that despite the obvious limitations of our model, it is capturing aspects of the essential dynamics in these experiments. And although there has been debate about whether a single neuron can undergo a “seizure” [12, 30], our single-neuron results suggest that ion concentration dynamics may well play an important role in epilepsy.

It is interesting to note that in order to obtain our type D burst, in which the burst termination transitions smoothly from depolarization block back to rest without exhibiting spikes (Fig. 4d), we found it necessary to increase the parameter  $\gamma$ , which is inversely proportional to the volume of our assumed spherical cell (see the Appendix). With a smaller volume, the internal sodium concentration is more easily increased to sufficient levels to

prevent spiking. Thus, our model predicts that this type of burst should be most easily observed in smaller neurons. Accordingly, this behavior has been seen in hippocampal interneurons (e.g., Fig. 4a of [29]). Similar behavior in other cases, however, may well be due to different mechanisms (e.g., calcium [31] or chloride accumulation [32]), and future work will explore the consequences of including these and other ions [33], as well as a more realistic collection of channels.

## 5 Conclusion

We have found that a simple model of a single neuron, augmented by dynamic intra- and extracellular ion concentrations, can display various kinds of periodic bursting behavior. Our work emphasizes the importance of ion concentration homeostasis in the maintenance of the normal physiological state and suggests that a breakdown in such homeostatic mechanisms may underlie pathological conditions such as epilepsy.

**Acknowledgements** The authors would like to acknowledge the assistance of Jeremy Owen in creating Fig. 2. This work was supported by the Collaborative Research in Computational Neuroscience program at National Institutes of Health via grant R01-MH79502 (EB).

## Appendix

Parameters and equations for gating variables

Parameters not specified above were set as follows:

$$\begin{aligned}C_m &= 1 \text{ } \mu\text{F}/\text{cm}^2 \\g_{\text{Na}} &= 100 \text{ mS}/\text{cm}^2 \\g_{\text{NaL}} &= 0.0175 \text{ mS}/\text{cm}^2 \\g_{\text{K}} &= 40 \text{ mS}/\text{cm}^2 \\g_{\text{KL}} &= 0.05 \text{ mS}/\text{cm}^2 \\g_{\text{CL}} &= 0.05 \text{ mS}/\text{cm}^2.\end{aligned}$$

The sodium activation was instantaneous, with

$$\begin{aligned}m_\infty(V) &= \frac{\alpha_m(V)}{\alpha_m(V) + \beta_m(V)} \\ \alpha_m(V) &= \frac{0.1(V + 30)}{1 - \exp(-0.1(V + 30))} \\ \beta_m(V) &= 4 \exp\left(-\frac{V + 55}{18}\right).\end{aligned}$$

The remaining gating variables were governed by

$$\frac{dq}{dt} = \phi [\alpha_q(V)(1 - q) - \beta_q(V)q], \quad q = h, n$$

with

$$\begin{aligned} \phi &= 3.0 \\ \alpha_h(V) &= 0.07 \exp\left(-\frac{V+44}{20}\right) \\ \beta_h(V) &= \frac{1}{1 + \exp(-0.1(V+14))} \\ \alpha_n(V) &= \frac{0.01(V+34)}{1 - \exp(-0.1(V+34))} \\ \beta_n(V) &= 0.125 \exp\left(-\frac{V+44}{80}\right). \end{aligned}$$

Derivation of conversion factors

To derive the conversion factor  $\gamma$ , we consider a membrane current density  $I$ , measured in  $\mu\text{A}/\text{cm}^2$ , and ask: how many ions exit a cell through a patch of membrane of area  $A$  (square centimeters) in time  $\Delta t$  (seconds) due to this current? Recalling the convention that membrane currents are positive outward, the amount of charge that leaves is

$$\Delta Q = (IA) \Delta t.$$

Assuming monovalent ions, the number of ions is

$$\Delta N = \left(\frac{IA}{q}\right) \Delta t,$$

where  $q = 1.60 \times 10^{-19}$  C. Hence, the rate at which ions pass through the area  $A$  is

$$\frac{dN}{dt} = \left(\frac{IA}{q}\right).$$

Now assume a spherical cell of volume  $V_{\text{in}}$  (measured in cubic centimeters) with an intracellular concentration  $c_{\text{in}}$  of positive ions measured in ions per cubic centimeter. We have

$$c_{\text{in}} = \frac{N}{V_{\text{in}}},$$

where  $N$  is the number of ions within the volume. Hence,

$$\frac{dc_{\text{in}}}{dt} = \left(\frac{1}{V_{\text{in}}}\right) \frac{dN}{dt} = -\frac{1}{V_{\text{in}}} \left(\frac{IA}{q}\right).$$

The minus sign has been introduced because a positive (outward) current corresponds to a decrease in the number of (positive) ions within the cell.

We wish to express this rate of change of concentration in millimolars per millisecond. The expression on the right-hand side has units

$$\frac{1}{\text{cm}^3} \frac{\frac{\mu\text{A}}{\text{cm}^2} \text{cm}^2}{\text{C}} \rightarrow 10^{-6} \frac{\text{ions}}{\text{cm}^3 \text{s}} \rightarrow \frac{1}{10^3 N_A} \frac{\text{mmol}}{\text{ms L}},$$

where  $N_A = 6.02 \times 10^{23}$  is Avogadro's number. Since  $1 \text{ mmol/L} = 1 \text{ mM}$ , we have

$$\frac{dc_{\text{in}}}{dt} = - \left( \frac{1}{10^3} \right) \frac{IA}{N_A q V_{\text{in}}}.$$

We write

$$\frac{dc_{\text{in}}}{dt} = - \left( \frac{1}{10^3} \right) \gamma I \quad (7)$$

with

$$\gamma \equiv \frac{A}{N_A q V_{\text{in}}} = \frac{A}{F V_{\text{in}}},$$

where  $F = N_A q$  is the Faraday constant. Equation 7 is used for the intracellular sodium in (4).

Now assume that the sphere has radius  $r$ , and let  $A$  be its total surface area. (More correct would be to let  $A$  be just the area of the channel pores.) Then,

$$\gamma = \frac{3}{Fr}.$$

Using  $r = 7 \text{ } \mu\text{m}$ , we obtain  $\gamma = 4.45 \times 10^{-2}$ . Conversely, for  $\gamma = 0.25$  and  $1.0$ , we obtain  $r = 1.24$  and  $0.31 \text{ } \mu\text{m}$ , respectively.

Consider now the concentration of positive ions in the extracellular space. The volume in the expression for  $\gamma$  must be replaced with the extracellular volume, and the negative sign in (7) must be removed. Let  $\beta \equiv V_{\text{in}}/V_{\text{out}}$ . Then  $\gamma \rightarrow \gamma\beta$ , and we have

$$\frac{dc_{\text{out}}}{dt} = \left( \frac{1}{10^3} \right) \gamma\beta I. \quad (8)$$

Equation 8 is used for the extracellular potassium in (4).

## References

1. Hodgkin, A.L., Huxley, A.F.: A quantitative description of membrane current and its application to conduction and excitation in nerve. *J. Physiol.* **117**(4), 500–544 (1952)
2. Frankenhaeuser, B., Hodgkin, A.L.: The after-effects of impulses in the giant nerve fibres of *Loligo*. *J. Physiol.* **131**, 341–376 (1956)
3. Grafstein, B.: Mechanism of spreading cortical depression. *J. Neurophysiol.* **19**, 154–171 (1956)
4. Green, J.D.: The hippocampus. *Phys. Rev.* **44**, 561–608 (1964)
5. Fetzinger, A.P., Ranck, J.B., Jr.: Potassium accumulation in interstitial space during epileptiform seizures. *Exp. Neurol.* **26**, 571–585 (1970)
6. Fröhlich, F., Bazhenov, M., Iragui-Madoz, V., Sejnowski, T.J.: Potassium dynamics in the epileptic cortex: new insights on an old topic. *Neurosci.* **14**(5), 422–433 (2008)
7. Kager, H., Wadman, W.J., Somjen, G.G.: Conditions for the triggering of spreading depression studied with computer simulations. *J. Neurophysiol.* **88**, 2700–2712 (2002)
8. Somjen, G.G., Kager, H., Wadman, W.J.: Calcium sensitive non-selective cation current promotes seizure-like discharges and spreading depression in a model neuron. *J. Comput. Neurosci.* **26**, 139–147 (2008)
9. Bazhenov, M., Timofeev, I., Steriade, M., Sejnowski, T.J.: Potassium model for slow (2–3 Hz) in vivo neocortical paroxysmal oscillations. *J. Neurophysiol.* **92**, 1116–1132 (2004)
10. Fröhlich, F., Bazhenov, M., Timofeev, I., Steriade, M., Sejnowski, T.J.: Slow state transitions of sustained neural oscillations by activity-dependent modulation of intrinsic excitability. *J. Neurosci.* **26**(23), 6153–6162 (2006)

11. Park, E.H., Durand, D.M.: Role of potassium lateral diffusion in non-synaptic epilepsy: a computational study. *J. Theor. Biol.* **238**, 666–682 (2006)
12. Kager, H., Wadman, W.J., Somjen, G.G.: Seizure-like afterdischarges simulated in a model neuron. *J. Comput. Neurosci.* **22**, 105–128 (2007)
13. Somjen, G.G., Kager, H., Wadman, W.J.: Computer simulations of neuron–glia interactions mediated by ion flux. *J. Comput. Neurosci.* **25**, 349–365 (2008)
14. Postnov, D.E., Müller, F., Schuppner, R.B., Schimansky-Geier, L.: Dynamical structures in binary media of potassium-driven neurons. *Phys. Rev. E* **80**, 031921 (2009)
15. Fröhlich, F., Sejnowski, T.J., Bazhenov, M.: Network bistability mediates spontaneous transitions between normal and pathological brain states. *J. Neurosci.* **30**(32), 10734–10743 (2010)
16. Kager, H., Wadman, W.J., Somjen, G.G.: Simulated seizures and spreading depression in a neuron model incorporating interstitial space and ion concentrations. *J. Neurophysiol.* **84**, 495–512 (2000)
17. Somjen, G.G.: *Ions in the Brain*. Oxford University Press, New York (2004)
18. Cressman, J.R., Ullah, G., Schiff, S.J., Barreto, E.: The influence of sodium and potassium dynamics on excitability, seizures, and the stability of persistent states: I. Single neuron dynamics. *J. Comput. Neurosci.* **26**, 159–170 (2009)
19. Dayan, P., Abbott, L.F.: *Theoretical Neuroscience*. MIT, Cambridge (2001)
20. Bikson, M., Hahn, P.J., Fox, J.E., Jefferys, J.G.R.: Depolarization block of neurons during maintenance of electrographic seizures. *J. Neurophysiol.* **90**, 2402–2408 (2003)
21. Izhikevich, E.: *Dynamical Systems in Neuroscience*. MIT, Cambridge (2007)
22. Martens, E., Barreto, E., Strogatz, S.H., Ott, E., So, P., Antonsen, T.M.: Exact results for the Kuramoto model with a bimodal frequency distribution. *Phys. Rev. E* **79**, 026204 (2009)
23. Shilnikov, A.L., Calabrese R., Cymbalyuk, G.S.: Mechanism of bi-stability: tonic spiking and bursting in a neuron model. *Phys. Rev. E* **71**, 056214 (2005)
24. Cymbalyuk, G.S., Calabrese R., Shilnikov, A.L.: How a neuron model can demonstrate co-existence of tonic spiking and bursting? *Neurocomputing* **65–66**, 869–875 (2005)
25. Fröhlich, F., Bazhenov, M.: Coexistence of tonic firing and bursting in cortical neurons. *Phys. Rev. E* **74**, 031922 (2006)
26. Guckenheimer, J., Holmes, P.: *Nonlinear Oscillations, Dynamical Systems, and Bifurcations of Vector Fields*. Springer, New York (1983)
27. Guckenheimer, J.: Multiple bifurcation problems for chemical reactors. *Physica D* **20**(1), 1–20 (1986)
28. Jensen, M.S., Yaari, Y.: Role of intrinsic burst firing, potassium accumulation, and electrical coupling in the elevated potassium model of hippocampal epilepsy. *J. Neurophysiol.* **77**, 1224–1233 (1997)
29. Ziburkus, J., Cressman, J.R., Barreto, E., Schiff, S.J.: Interneuron and pyramidal cell interplay during in vitro seizure-like events. *J. Neurophysiol.* **95**, 3948–3954 (2006)
30. Connors, B.W., Telfeian, A.E.: Dynamic properties of cells, synapses, circuits and seizures in neocortex. In: Williamson, P.D., et al. (eds.) *Neocortical Epilepsies*. *Advances in Neurology*, vol. 84, pp. 141–152 (2000)
31. Pinsky, P.F., Rinzel, J.: Intrinsic and network rhythmogenesis in a reduced Traub model for CA3 neurons. *J. Comput. Neurosci.* **1**, 39–60 (1994)
32. Marchetti, C., Tabak, J., Chub, N., O’Donovan, M.J., Rinzel, J.: Modeling spontaneous activity in the developing spinal cord using activity-dependent variations of intracellular chloride. *J. Neurosci.* **25**(14), 3601–3612 (2005)
33. Komendantov, A., Cressman, J.R., Barreto, E.: Ion concentration homeostasis and the regulation of neuronal firing activity: the role of cation-chloride cotransporters. *BMC Neurosci.* **11**(Suppl 1), P27 (2010)